Advances in Cryo-ET and Subtomogram Averaging

Lorenzo Gaifas

Examiner: Cristina Paulino

August 5, 2020

Abstract

Cryo Electron Tomography (Cryo-ET) — which stems from the better known Cryo Electron Microscopy — is a powerful imaging technique that allows for high resolution structure determination of single samples in native conformation or *in situ*. Recent engineering and computational advances brought Cryo-ET back to the front-line of structural biology, opening up new applications and possibilities. Here, we describe the state of the art of Cryo-ET, with a particular focus on subtomogram averaging for single particle studies, and explore the recent technological advances that prove most promising for the future of this technique.

Contents

1 Introduction

Interactions between biological molecules are heavily dependent on their structural features. The goal of structural biology is to understand the function of such molecules by determining and understanding their three-dimensional structure.

Structural biologists employ a few different methods to this end; the most commonly used techniques for structure determination are X-ray crystallography, NMR and Electron Microscopy (EM). Currently, these techniques respectively account for about 89%, 8% and 3% of PDB entries[1].

Despite its spread, X-ray crystallography is limited by its applicability to molecular complexes, and relies on the capability of the target molecule to form crystals. Less diffused than X-ray crystallography, structure determination through NMR is very powerful, but can only be applied to relatively small systems due to the high complexity of the information and other effects of bigger systems such as slower tumbling.

Cryo Electron Microscopy (Cryo-EM) is the least common of the three techniques, but has been slowly gaining traction in the structural biology community. Cryo-EM is a well-established imaging technique which consists in imaging cryogenically vitrified samples with an electron microscope. It appears in published papers as far back as 70 years ago, which test and discuss its potential for structure determination[2].

In recent years, advances in both engineering and computational equipment led to new advances in Cryo-EM which brought this technique back to the front-line of structural biology research. Where it was once impractical or inferior to existing alternatives, Cryo-EM is now approaching the high resolution of X-ray crystallography, while proving more versatile and being applicable to new and different studies[3].

1.1 Single-particle Cryo-EM

The most common application of Cryo-EM is single-particle structure determination[4,5], which is often chosen as an alternative to X-ray crystallography for the structural study of proteins and other biological macromolecules.

In single-particle analysis (SPA), samples of purified molecules are applied to a specialized grid in order to form a thin layer, which is then vitrified by plunge-freezing. The process of vitrification preserves the native structure of the samples, while limiting the effects of radiation damage[6]. Such samples are then imaged using an electron microscope; the resulting images are 2D projections of several copies of the target molecule in many different orientations. Images are then computationally combined into a 3D reconstruction

of the target, which can be interpreted in a similar way to electron-density maps obtained through X-ray crystallography.

1.1.1 Advantages over X-ray crystallography

Differently from X-ray crystallography, Cryo-EM does not require to crystallize the target prior to imaging; instead, samples are vitrified by rapid freezing. This not only makes sample preparation less complicated, but also fixates the target in a near-native conformation, preserving features that may otherwise be lost or altered during the crystallization process. By not restricting the conformational space of the target to be crystal-compliant, Cryo-EM also allows for structure determination of challenging targets — such as integral membrane proteins of mammal origin or chromatin in complex with its modifiers — which would otherwise be near impossible with X-ray crystallography.

While SPA presents several benefits over X-ray crystallography, it also maintains some of the same disadvantages. One such limitation is due to the necessity of imaging many copies of the target arranged in a grid in different orientations, which precludes the analysis of samples *in situ* and of systems of disordered nature.

Here, we focus on a branch of Cryo-EM called Cryo Electron Tomography (Cryo-ET), which opened new possibilities by allowing for high resolution *in situ* structure determination[7].

1.2 Cryo Electron Tomography

Cryo Electron Tomography (Cryo-ET) is a technique used to reconstruct a 3D image of a vitrified biological sample *in situ*. This is achieved by acquiring a set of projection images of the sample from several different orientations (tilt series), which are then computationally combined to reconstruct the 3D structure of the target (tomogram).

This approach provides a mean to inspect structural features of complex systems that cannot be imaged with other methods because they cannot be crystallized nor purified to a simple elementary unit.

To extract the most information from a tomographic reconstruction, subtomogram averaging (StA) can be be used when several copies of the target particle are present in one (or more) tomograms. By extracting the subtomograms containing each particle, aligning them and averaging their density maps, it is possible to dramatically increase the resolution of the reconstructed 3D particle.

While Cryo-ET is an old technique, recent developments in data acquisition and processing show promising advancements in its applications and capabilities for the near future. The following sections describe the state of the art of Cryo-ET, analyzing the future perspectives for each step of this imaging technique, from sample preparation to tomogram reconstruction and subtomogram averaging.

2 Sample preparation

The first challenges in Cryo-ET imaging come from the preparation of samples. Several optimizations in this step can improve the quality of the data, simplify the imaging process or allow for different targets.

2.1 Vitrification

Samples are vitrified for a few reasons: to preserve their structure, to improve their resistance to the high energy of the electron beam, and to protect them from the vacuum needed for EM imaging.

Vitrification is can be achieved through High Pressure Freezing[8] or Plunge Freezing[9]; these procedures are designed to cool down the samples extremely rapidly in order to prevent the formation of ice crystals, which can damage and deform dramatically the structure of the target.

Vitrification is a complex procedure that, if done manually, can lead to suboptimal results that hurt reproducibility. While automated procedures exist, currently available robots still require a fair amount of manual intervention. A few improvements to the established vitrification techniques are currently under development: the use of new plunge freezing robots and nanowire grids can boost reproducibility and lower the dwell time of samples in thin liquid films, thus preventing the samples from adopting preferred orientations[10,11].

2.2 Slicing and Milling

One of the strength of Cryo-ET — the ability to image complex and heterogeneous systems — is also what requires additional care. Cells, organelle complexes, and other macromolecular structures are sometimes too thick for electron microscopy.

Imaging in EM depends on the elastic scattering of electrons; higher sample thickness means that a higher percentage of electrons gets scattered inelastically, effectively losing information while damaging the sample. This

imposes a practical limit for Cryo-ET sample thickness at around 300 nm, which amounts to an apparent thickness of ∼600 nm at high tilt angles[12].

Due to this limitations, naturally thick samples such as cells need to be thinned before they can be imaged by Cryo-ET. Currently, the most established thinning approach is Cryo-sectioning, also called CEMOVIS; samples are simply cut with a diamond knife before being deposited on the EM grid[13]. However, CEMOVIS is a very low throughput technique that inevitably deforms the sample with compression, and formation of crevasses and breaks in the ice[14].

In recent years, cryo-sectioning started to give way to more modern technologies, such as focused ion beam (FIB) milling[14,15]. Instead of cutting the sample, FIB milling progressively removes material from the ice layer by bombarding it with Ga^{3+} ions. Differently from CEMOVIS, this technique preserves the sample to a near-native condition.

Although FIB milling is not yet widespread, as it requires highly specialized equipment, it already enabled novel *in situ* structural insights as well as providing a new perspective on the dynamic nature of cellular complexes[16].

Despite the benefits, FIB milling does not improve on one of CEMOVIS limitations: with both techniques, it is hard to cut the sample to the desired thickness while maintaining the feature of interest inside the ice layer. Currently, this is solved by collecting low-dose EM images to determine the position of the target feature inside the ice layer; this method, however, is limited by the poor contrast of EM images, especially when trying to minimize the exposure of the sample to harmful radiation.

A better approach, though still relatively immature, is correlative microscopy: by using fluorescence microscopy to more easily detect sample features, it is possible to find and focus the region of interest with the electron microscope, with more accuracy and without damaging the sample in the process[17].

2.3 Fiducial markers

Images within a tilt series require careful alignment before performing the tomographic reconstruction. Despite the engineering advances in the automated collection of tilt series and fiducialless alignment procedures, the use of fiducial markers such as gold beads is still extremely helpful for the proper alignment of a tilt series (Figure 1).

Fiducials are added to the samples before vitrification; the high contrast of the fiducial markers against the surroundings allows for higher precision in the tilt series alignment process (see Section 4.2).

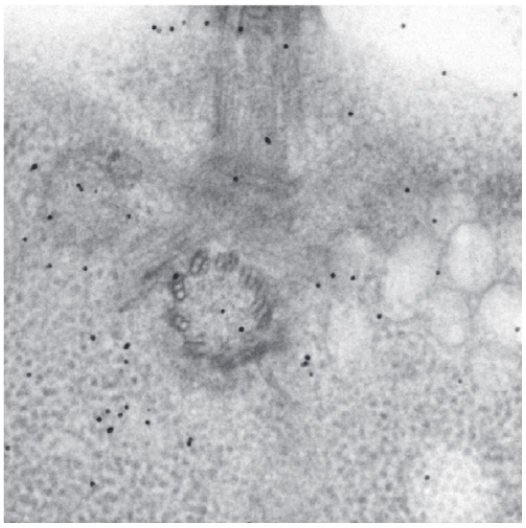

Figure 1: *EM projection image of a sample containing gold bead fiducials. Fiducials are visible as small dark disks with high contrast to the surroundings.*

3 Data acquisition

One of the main limitations in Cryo-EM is the intrinsically low signal to noise ratio (SNR). This is further complicated by the progressive degradation of the sample due to the high energy of the electron beam. This is particularly problematic for Cryo-ET, since a single sample needs to be imaged multiple times during the collection of a tilt series. Due to this effect, there is a practical limit to how much information can be extracted from a given sample.

To compensate these limitations, during data acquisition particular care must be taken to reduce secondary sources of noise and minimize the effects of sample degradation.

3.1 Collection schemes

As mentioned in section 2.2, higher sample thickness leads to higher inelastic scattering, and therefore worse quality images. Higher resolution information is the first to be lost to this phenomenon.

In Cryo-ET, imaging a sample at higher tilts is effectively equivalent to imaging a thicker sample. Due to this reason, most of the high resolution information is found at low tilts. Since high resolution information is also the first to be degraded by radiation damage, an ideal tilt series should be collected first at low tilt angles, progressively moving towards higher tilts.

Conventionally, tilt series are collected along two passes: from 0°to +60°, and then from 0°to –60°). Though this bi-directional tilt scheme is better than the older, continuous method, more recent microscope mounts and software enable the use of a dose-symmetric collection scheme[18]. This improved collection method maximizes the high-resolution information collected in early images, thus minimizing the impact of sample degradation (Figure 2). Additionally, it distributes the radiation damage more evenly throughout the tilt series, which later improves tilt series alignment.

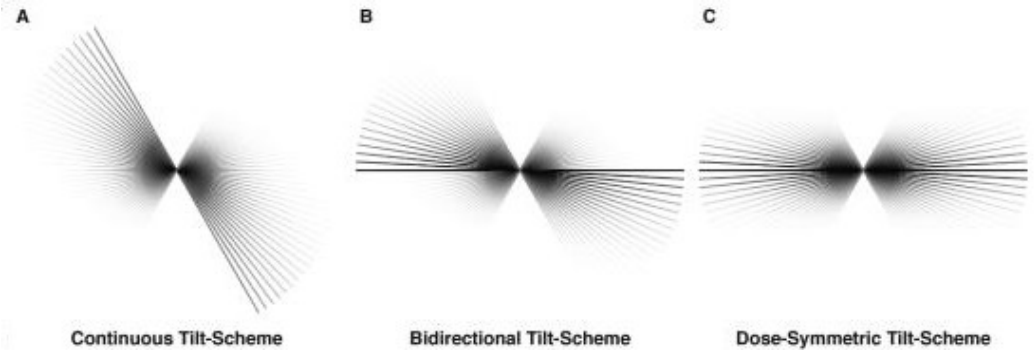

Figure 2: *Schematic representation of different collection schemes. Darker lines represent early images, while lighter lines represent later images. In the continuous tilt scheme (**A**), high-resolution information is already severely degraded before reaching the lower tilts. In the bidirectional tilt scheme (**B**), the first pass starts from zero tilt, collecting more high resolution information than the continuous tilt scheme. The dose-symmetric tilt-scheme (**C**) concentrates all the first images at lower tilts, retaining the most high resolution information against sample degradation. Figure taken from Hagen et Al.*[18].

The speed of data collection can also be significantly impacted by the collection scheme and imaging procedures. Through automation, it is possible to increase the precision of mechanical movements, as well as speeding up the imaging process.

The relatively slow speed of data collection currently poses a significant limit to the throughput of a single microscope. Conventional tilt series acquisition can typically take between 20 and 60 minutes, mostly due to unstable mechanical movements which require automated tracking and focusing to compensate between each imaging step.

New tilting schemes, such as the "fast-incremental single-exposure" (FISE) method, promise to remove these additional steps and increase imaging speed several-fold[19]. FISE eliminates a lot of idle camera time by collecting a continuous movie of the sample with a blanked beam. At discrete tilt angles, the electron beam is unblanked to record an actual image for the tilt series.

3.2 Detectors

Electron microscopes collect information by means of a detector, or camera. Older microscopes used photographic film for this purpose. While capable of recording very high resolution images, this type of detector has a low throughput and does not lend itself easily to automation, due to the several steps needed to develop the image and access the data.

CCD-based detectors — currently the most common type of camera — provide instead immediate access to the collected data, while also offering higher dynamic range[20,21]. They work by first converting incident electrons into light, which is then detected by the CCD. However, the converted light suffers from scattering, which lowers the practical resolution limit that can be reached by this method. Moreover, due to charge sharing between pixels, CCD detectors have relatively low SNR, which makes them particularly unsuitable for Cryo-ET.

In the last decade, wider use of Direct Detector Devices (DDD) significantly improved the quality of collected data. Differently from CCD, DDD bypass the conversion step and offer higher SNR, better resolution, and have better Detective Quantum Efficiency (DQE) and Modulation Transfer Function (MTF) for Cryo-EM and Cryo-ET than their predecessors[22,23].

Recent improvements in DD such as the Gatan K3 were shown to further speed up data collection in combination with collection methods like FISE by effectively eliminating most of the processing time during imaging[24].

4 Image processing

After imaging, the acquired data must undergo a series of processing steps before it can be used to reconstruct the sample.

The main issues that data processing tries to solve are defocus, tilt series alignment, and the missing wedge.

4.1 Defocus determination and Contrast Transfer Function

The Contrast Transfer Function (CTF) describes the signal transfer at different spacial frequencies, and is determined by the physical properties of the microscope, as well as other parameters such as electron voltage, acceleration voltage and defocus. Due to these properties and electron interference, the signal transfer changes periodically based on the spacial frequency, resulting in zeroes that manifest in Fourier space in the form of Thon rings (Figure 3).

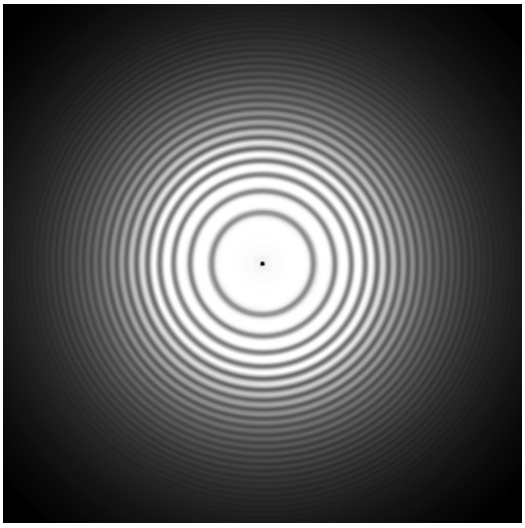

Figure 3: *Illustration of how Thon rings may appear in Fourier space. Low spacial frequencies are at the center of the image, while high frequencies are at the edges. Where Thon rings reach zero intensity, information is completely and irretrievably lost to destructive interference. In areas surrounding these zeroes, however, information is only attenuated and can be recovered through CTF correction.*

One of the parameters that greatly affect the CTF is the defocus value, which is determined by the distance between the focal plane of the microscope and the target particle. Calculating the defocus value for a given image (or image patch) is essential to apply a CTF correction and compensate for this problem.

This is more difficult in tomography than in single particle Cryo-EM, as in a tilted specimen there is a defocus gradient perpendicular to the tilt axis. Typically, this is solved by calculating strip-wise defoci along the gradient and performing CTF correction on each strip[25,26].

Another complication is introduced by thicker specimens, where individual particles can be found at significantly different Z positions, requiring CTF correction to be thickness-sensitive. A solution to this problem can be found in 3D CTF correction[27–30], or in determining the local defocus of each particle in order to perform particle-wise CTF correction[31].

Novel approaches and algorithms to further improve defocus determination and CTF correction are being developed every year, such as faster and more accurate computational tools and algorithms[32,33].

4.2 Tilt series alignment

As previously mentioned in section 2.3, the most common and effective method for tilt series alignment is the use of gold beads as fiducials.

Fiducials appear as high contrast dots embedded in the ice layer. They provide easily trackable features that can be used to estimate sample displacement and stage drift. By aligning the position of fiducials throughout the tilt series, the alignment of the samples themselves is significantly improved.

Human intervention is often required to ignore or manually identify fiducials that migrate during data collection or overlap with other fiducials at a different depth. To solve this problem, automated alignment procedures that require almost no human intervention have recently been published, and achieved equally good results as traditional semi-automated techniques[34]. This proves useful especially for StA, which would benefit greatly from batch image processing.

While fiducials are relatively easily embedded in *in vitro* samples, the use of fiducials *in situ* is sometimes hard or undesirable. Although less accurate than their fiducial-based counterparts, non-fiducial-based alignment approaches are available: for example, by calculating the cross-correlation (CC) between image patches in a tilt series[35].

4.3 The missing wedge

Tilt series acquisition is limited by the sample holder geometry and the thickness of the sample. As a result, the maximum tilt angle that can be collected is less than the full 90°(usually collection stops at around 60°).

Since 3D reconstruction relies on the projection images collected in a tilt series in order to fill the Fourier space (see section 6 for more detail on tomographic reconstruction), an incomplete tilt series results in an incomplete Fourier space. This limitation results in the so-called *missing wedge*, a wedge-shaped region in the spacial frequency domain which is void of information. In real space, this results in smearing of the density map (Figure 4).

This issue is especially problematic for StA, where subvolumes containing a target particle must be aligned to each other. The zeros that compose the missing wedge in Fourier space overpower every other feature when performing the cross-correlation (CC) search needed for subtomogram alignment.

This can be solved by using a Fourier space CC procedure which properly weighs zeroes in the search[36,37]. With similar results, thresholding CC simply ignores the lower Fourier coefficients, thus discarding the missing wedge and most of the noise[38,39].

Very different approaches attempt to completely remove the missing wedge

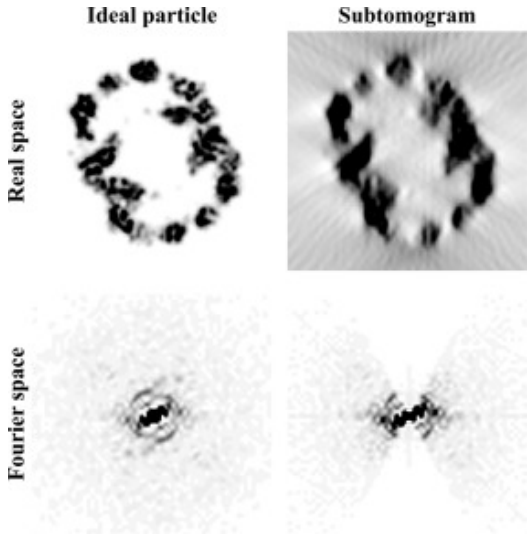

Figure 4: *Example of missing wedge and its effect on the subtomogram of a particle. The left column shows a complete, simulated density map without missing wedge. On the right is instead the same density map reconstructed through a simulated tilt series (-60°to 60°, with 3°increments). The bottom right figure shows the missing wedge in Fourier space. The top right one shows its effects in real space. Figure taken from Wan and Briggs*[31]*.*

problem by using FIB to mill the sample to an ice needle, or using a cylindrical sample holder[40–42].

5 Denoising

As the low SNR poses the main limitation to quality of Cryo-ET reconstructions, it comes to no surprise that a need for advanced denoising techniques is increasingly more widespread in the tomography community.

Conventional denoising in Cryo-EM and Cryo-ET is obtained through filters based on the local image context, such as non-linear anisotropic diffusion filters[43], bilateral filters[44], and iterative median filters[45].

These techniques, while improving on the older and more trivial low-pass filtering in different ways, still rely on the local neighbourhood of each pixel to determine its intensity. More recent, non-local filtering approaches use a much wider range of pixels, significantly improving the detail retention while performing as well as local filters for noise removal[46].

The rapid advancement of Machine Learning (ML) methods for data denoising offers entirely new possibilities for Cryo-ET. A recently published image restoration technique known as noise2noise (N2N) seems particularly

promising for tomography[47]. In conventional ML denoising techniques, neural network training requires a dataset of pairs of high and low quality images. In Cryo-ET, however, it is virtually impossible to obtain noise-free data; N2N provides a mean to circumvent this necessity.

N2N works based on the idea that *corrupting the training data of a neural network with a zero-mean noise won't change the output of the network*. Thus, in order to train the N2N neural network, many independently noisy but otherwise equal image pairs are collected and then compared by the network, which is able to effectively learn how a noisy image can be converted into the same image, but with different noise. The average between them is, in practice, the noise-free image.

Some publications applying this technique to Cryo-ET already appeared, such as cryo-CARE[48], which combines content-aware image restoration with a N2N-trained neural network. Similarly, Topaz-Denoise implements a noise2noise-based denoising procedure, trained over thousands of micrographs in varying conditions, thus providing a general-purpose tool without necessitating re-training on a per-dataset base[49].

6 Tomographic reconstruction

After processing, the tilt series can finally be used to reconstruct a 3D tomogram. This reconstruction is usually performed through Fourier synthesis. According to the central slice theorem, the Fourier transform of each 2D projection image in the tilt series corresponds to a central slice through the 3D Fourier transform of the real object. By collecting a tilt series, it is possible to partially fill the 3D Fourier space, which can then be inverse transformed back to 3D real space (Figure 5).

WBP is one of the most commonly used techniques, as it is less computationally intensive than Fourier synthesis but for many applications practically analogous. However, depending on the weighing function used, WBP can lead to a loss of contrast; this can result in poorer subtomogram alignment precision, and hinders particle identification[51].

On the other hand, iterative methods improve contrast retention compare to WPB, but take significantly longer to reach convergence. Additionally, they can be prone to loss of high resolution signal, which is essential for good quality StA[31,51].

New iterative algorithms with a focus on StA (such as INFR[52], ICON[53] and supersampling SART[54]) were recently developed, but are not yet established as good replacements to WBP and Fourier synthesis.

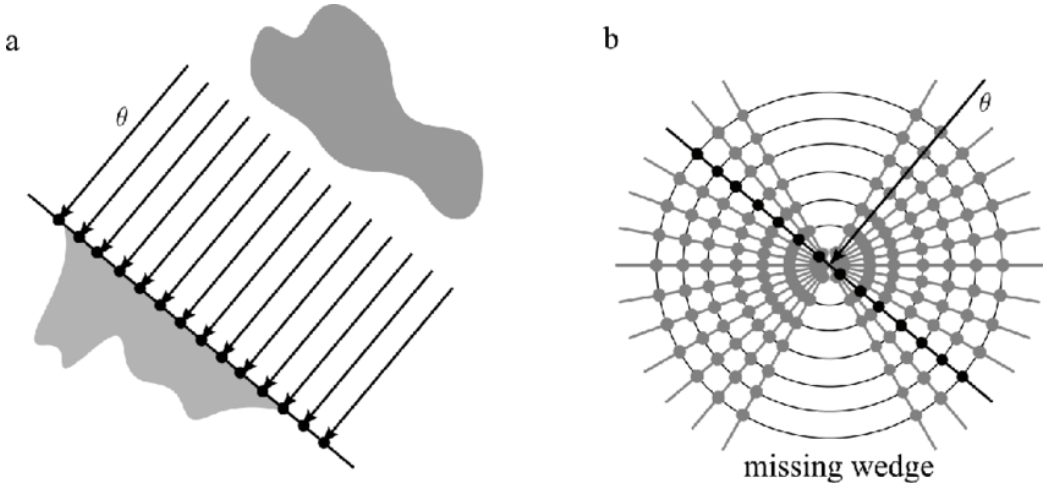

Figure 5: *Schematic representation of the Fourier slice theorem. A slice is obtained by imaging the sample in direction θ, resulting in a 2D projection image (**A**). The Fourier transform of that projection corresponds to a single central slice in Fourier 3D space at angle θ (**B**). The missing wedge is a region of Fourier space where information is missing, due to the limited tilt that can be reached by the sample. Figure taken from Dahmen et Al.*[50].

6.1 Subtomogram Averaging

In order to perform averaging over the density map of several particles, subtomograms need to be first identified and aligned. Additionally, clustering and classification of subtomograms is necessary to distinguish between slightly different particles or conformations.

6.1.1 Template matching

Template matching uses an exhaustive search where a template density map is translated and rotated through the full 3D space, and then compared at each position to measure the similarity to the tomogram. A similarity score is then calculated and normalized for each position in the tomogram, with high scores indicating a recognized particle[55].

While this method has been put extensively to good use, it has several flaws, first and foremost the need of a template of known structure. While it is possible to compare databases of different templates, this is computationally inefficient, still requires a "complete" database and is not suited for matching complexes.

Moreover, due to overfitting and the use of a mostly arbitrary cutoff for similarity, the template is always recovered (template bias), and if the same

similarity criteria are then used for cross-validation, true and false positives are virtually indistinguishable[56].

6.1.2 Reference-free alignments

The *ab initio* Stochastic Gradient Descent (SGD) algorithm introduced in cryoSPARC is an optimization technique that begins with a randomly initialized map which is iteratively improved through many noisy steps. This technique can solve some of the problems of template matching; it eliminates the need for a known template, while introducing some precautions against overfitting[57].

Other reference-free approaches include Fourier space constrained volumetric matching[58], and local feature enhancement, which reduce the influence of noise and enhance important features through the application of a weight mask[58].

Recently, a procedure for template-free tracing and alignment called PySeg was developed based on the discrete Morse theory[59]. PySeg was effectively used to automatically and comprehensively detect heterogeneous, membrane-bound complexes on the endoplasmic reticulum.

Recent publications showed how the use of Machine Learning (ML) can significantly improve particle recognition and classification, while not requiring *a priori* knowledge of the target.

First attempts at using Convolutional Neural Networks (CNN) in Cryo-EM SPA showed a similar performance to conventional template-matching[60]. Further improvements were obtained through the use of deep residual networks such as BoxNet used by Warp[61].

Another application of a CNN by Chen et Al.[62] uses a slice-wise approach which greatly simplifies the complexity of the Neural Network, and can be easily re-trained for specific features with a small dataset of manually annotated images.

Deep Learning is also used by crYOLO[14,63], which uses the You Only Look Once object detection framework to pick particles in a low SNR tomogram.

A different Neural Network is used by KerDenSOM3D[56], a 3D implementation of the "Kernel Density Estimator Self–Organizing Map", which classifies subtomograms by reducing the dataset to a small set of good-quality representatives.

7 Discussion

In the last few years, Cryo-ET techniques underwent steady improvements both on the engineering and computational front. In particular, new tools and methods of great importance for subtomogram averaging have been developed, such as direct detectors and machine learning-based reference-free template matching and denoising. All these new methods contribute to overcome the biggest limitation of StA: the extremely low SNR and subsequent difficulty to obtain high resolution structures.

New direct detectors in combination with clever collection techniques — such as the Gatan K3-FISE combination[24] — significantly reduce the collection time of Cryo-ET. This enables easier and more effective automation for routines such as StA, which require long experimental measurements times and produce high volumes of raw data.

The massive surge in new machine learning technologies will also play a major role in Cryo-ET development, with techniques such as template matching[56,60–62,64] and image denoising[48,49] already showing the first promising results in this field .

As several of these tools and techniques are currently still limited in scope and applicability, we expect that future research will focus on refining, automating and implementing them in mainstream Cryo-ET hardware and software. The improvements brought by these new tools extends the applicability of Cryo-ET to new molecular complexes, more heterogeneous, smaller, and rarer than previously possible, making structure determination of large, complexm, and dynamic systems *in situ* a more concrete possibility.

References

[1] RCSB Protein Data Bank. RCSB PDB. https://www.rcsb.org/stats/summary. (3)

[2] H. Fernández-Morán. The submicroscopic organization of vertebrate nerve fibres: An electron microscope study of myelinated and unmyelinated nerve fibres. *Experimental Cell Research*, 3(2):282–359, January 1952. (3)

[3] Carol V. Robinson, Andrej Sali, and Wolfgang Baumeister. The molecular sociology of the cell. *Nature*, 450(7172):973–982, December 2007. (3)

[4] Joachim Frank. Single-Particle Imaging of Macromolecules by Cryo-Electron Microscopy. *Annual Review of Biophysics and Biomolecular Structure*, 31(1):303–319, 2002. _eprint: https://doi.org/10.1146/annurev.biophys.31.082901.134202. (3)

[5] Yifan Cheng. Single-Particle Cryo-EM at Crystallographic Resolution. *Cell*, 161(3):450–457, April 2015. (3)

[6] Holger Stark, Friedrich Zemlin, and Christoph Boettcher. Electron radiation damage to protein crystals of bacteriorhodopsin at different temperatures. *Ultramicroscopy*, 63(2):75–79, June 1996. (3)

[7] Vladan Lučić, Alexander Rigort, and Wolfgang Baumeister. Cryo-electron tomography: The challenge of doing structural biology in situ. *J Cell Biol*, 202(3):407–419, August 2013. (4)

[8] Daniel Studer, Bruno M. Humbel, and Matthias Chiquet. Electron microscopy of high pressure frozen samples: Bridging the gap between cellular ultrastructure and atomic resolution. *Histochem Cell Biol*, 130(5):877–889, November 2008. (5)

[9] Jacques Dubochet, Marc Adrian, Jiin-Ju Chang, Jean-Claude Homo, Jean Lepault, Alasdair W. McDowall, and Patrick Schultz. Cryo-electron microscopy of vitrified specimens. *Quarterly Reviews of Biophysics*, 21(2):129–228, May 1988. (5)

[10] Ivan Razinkov, Venkata P. Dandey, Hui Wei, Zhening Zhang, David Melnekoff, William J. Rice, Christoph Wigge, Clinton S. Potter, and Bridget Carragher. A new method for vitrifying samples for cryoEM. *Journal of Structural Biology*, 195(2):190–198, August 2016. (5)

[11] Stefan A. Arnold, Stefan Albiez, Andrej Bieri, Anastasia Syntychaki, Ricardo Adaixo, Robert A. McLeod, Kenneth N. Goldie, Henning Stahlberg, and Thomas Braun. Blotting-free and lossless cryo-electron microscopy grid preparation from nanoliter-sized protein samples and single-cell extracts. *Journal of Structural Biology*, 197(3):220–226, March 2017. (5)

[12] Radostin Danev, Haruaki Yanagisawa, and Masahide Kikkawa. Cryo-Electron Microscopy Methodology: Current Aspects and Future Directions. *Trends Biochem. Sci.*, 44(10):837–848, October 2019. (6)

[13] Ashraf Al-Amoudi, Jiin-Ju Chang, Amélie Leforestier, Alasdair McDowall, Laurée Michel Salamin, Lars PO Norlén, Karsten Richter, Nathalie Sartori Blanc, Daniel Studer, and Jacques Dubochet. Cryo-electron microscopy of vitreous sections. *The EMBO Journal*, 23(18):3583–3588, September 2004. (6)

[14] Jonathan Wagner, Miroslava Schaffer, and Rubén Fernández-Busnadiego. Cryo-electron tomography-the cell biology that came in from the cold. *FEBS Lett*, 591(17):2520–2533, September 2017. (6, 15)

[15] Michael Marko, Chyongere Hsieh, Richard Schalek, Joachim Frank, and Carmen Mannella. Focused-ion-beam thinning of frozen-hydrated biological specimens for cryo-electron microscopy. *Nat Methods*, 4(3):215–217, March 2007. (6)

[16] Stefan Pfeffer and Julia Mahamid. Unravelling molecular complexity in structural cell biology. *Current Opinion in Structural Biology*, 52:111–118, October 2018. (6)

[17] Anna Sartori, Rudolf Gatz, Florian Beck, Alexander Rigort, Wolfgang Baumeister, and Juergen M. Plitzko. Correlative microscopy: Bridging the gap between fluorescence light microscopy and cryo-electron tomography. *Journal of Structural Biology*, 160(2):135–145, November 2007. (6)

[18] Wim J.H. Hagen, William Wan, and John A.G. Briggs. Implementation of a cryo-electron tomography tilt-scheme optimized for high resolution subtomogram averaging. *J Struct Biol*, 197(2):191–198, February 2017. (8)

[19] Georges Chreifi, Songye Chen, Lauren Ann Metskas, Mohammed Kaplan, and Grant J. Jensen. Rapid tilt-series acquisition for electron cry-

otomography. *Journal of Structural Biology*, 205(2):163–169, February 2019. (8)

[20] A. R. Faruqi and Sriram Subramaniam. CCD detectors in high-resolution biological electron microscopy. *Quart. Rev. Biophys.*, 33(1):1–27, February 2000. (9)

[21] Kenneth H. Downing and Felicia M. Hendrickson. Performance of a 2k CCD camera designed for electron crystallography at 400kV. *Ultramicroscopy*, 75(4):215–233, January 1999. (9)

[22] G. McMullan, S. Chen, R. Henderson, and A. R. Faruqi. Detective quantum efficiency of electron area detectors in electron microscopy. *Ultramicroscopy*, 109(9):1126–1143, August 2009. (9)

[23] Rachel S. Ruskin, Zhiheng Yu, and Nikolaus Grigorieff. Quantitative characterization of electron detectors for transmission electron microscopy. *Journal of Structural Biology*, 184(3):385–393, December 2013. (9)

[24] Fabian Eisenstein, Radostin Danev, and Martin Pilhofer. Improved applicability and robustness of fast cryo-electron tomography data acquisition. *Journal of Structural Biology*, 208(2):107–114, November 2019. (9, 16)

[25] J. J. Fernández, S. Li, and R. A. Crowther. CTF determination and correction in electron cryotomography. *Ultramicroscopy*, 106(7):587–596, May 2006. (10)

[26] Quanren Xiong, Mary K. Morphew, Cindi L. Schwartz, Andreas H. Hoenger, and David N. Mastronarde. CTF determination and correction for low dose tomographic tilt series. *Journal of Structural Biology*, 168(3):378–387, December 2009. (10)

[27] Grant J Jensen and Roger D Kornberg. Defocus-gradient corrected back-projection. *Ultramicroscopy*, 84(1):57–64, July 2000. (10)

[28] Lenard M. Voortman, Sjoerd Stallinga, Remco H. M. Schoenmakers, Lucas J. van Vliet, and Bernd Rieger. A fast algorithm for computing and correcting the CTF for tilted, thick specimens in TEM. *Ultramicroscopy*, 111(8):1029–1036, July 2011.

[29] Lenard M. Voortman, Erik M. Franken, Lucas J. van Vliet, and Bernd Rieger. Fast, spatially varying CTF correction in TEM. *Ultramicroscopy*, 118:26–34, July 2012.

[30] Tanmay A.M. Bharat, Christopher J. Russo, Jan Löwe, Lori A. Passmore, and Sjors H.W. Scheres. Advances in Single-Particle Electron Cryomicroscopy Structure Determination applied to Sub-tomogram Averaging. *Structure*, 23(9):1743–1753, September 2015. (10)

[31] W. Wan and J. A. G. Briggs. Chapter Thirteen - Cryo-Electron Tomography and Subtomogram Averaging. In R. A. Crowther, editor, *Methods in Enzymology*, volume 579 of *The Resolution Revolution: Recent Advances In cryoEM*, pages 329–367. Academic Press, January 2016. (10, 12, 13)

[32] Alexis Rohou and Nikolaus Grigorieff. CTFFIND4: Fast and accurate defocus estimation from electron micrographs. *Journal of Structural Biology*, 192(2):216–221, November 2015. (10)

[33] Kai Zhang. Gctf: Real-time CTF determination and correction. *Journal of Structural Biology*, 193(1):1–12, January 2016. (10)

[34] Renmin Han, Liansan Wang, Zhiyong Liu, Fei Sun, and Fa Zhang. A novel fully automatic scheme for fiducial marker-based alignment in electron tomography. *Journal of Structural Biology*, 192(3):403–417, December 2015. (11)

[35] Fernando Amat, Daniel Castaño-Diez, Albert Lawrence, Farshid Moussavi, Hanspeter Winkler, and Mark Horowitz. Alignment of Cryo-Electron Tomography Datasets. In *Methods in Enzymology*, volume 482, pages 343–367. Elsevier, 2010. (11)

[36] Michael F. Schmid and Christopher R. Booth. Methods for aligning and for averaging 3D volumes with missing data. *Journal of Structural Biology*, 161(3):243–248, March 2008. (11)

[37] Michael F. Schmid. Single-particle electron cryotomography (cryoET). In *Advances in Protein Chemistry and Structural Biology*, volume 82, pages 37–65. Elsevier, 2011. (11)

[38] Fernando Amat, Luis R. Comolli, Farshid Moussavi, John Smit, Kenneth H. Downing, and Mark Horowitz. Subtomogram alignment by adaptive Fourier coefficient thresholding. *Journal of Structural Biology*, 171(3):332–344, September 2010. (11)

[39] Jesús G. Galaz-Montoya, Corey W. Hecksel, Philip R. Baldwin, Eryu Wang, Scott C. Weaver, Michael F. Schmid, Steven J. Ludtke, and Wah

Chiu. Alignment algorithms and per-particle CTF correction for single particle cryo-electron tomography. *Journal of Structural Biology*, 194(3):383–394, June 2016. (11)

[40] Zineb Saghi, Giorgio Divitini, Benjamin Winter, Rowan Leary, Erdmann Spiecker, Caterina Ducati, and Paul A. Midgley. Compressed sensing electron tomography of needle-shaped biological specimens – Potential for improved reconstruction fidelity with reduced dose. *Ultramicroscopy*, 160:230–238, January 2016. (12)

[41] Kedar Narayan, Ty J. Prosa, Jing Fu, Thomas F. Kelly, and Sriram Subramaniam. Chemical mapping of mammalian cells by atom probe tomography. *Journal of Structural Biology*, 178(2):98–107, May 2012.

[42] Colin M. Palmer and Jan Löwe. A cylindrical specimen holder for electron cryo-tomography. *Ultramicroscopy*, 137:20–29, February 2014. (12)

[43] Achilleas S. Frangakis and Reiner Hegerl. Noise Reduction in Electron Tomographic Reconstructions Using Nonlinear Anisotropic Diffusion. *Journal of Structural Biology*, 135(3):239–250, September 2001. (12)

[44] Wen Jiang, Matthew L Baker, Qiu Wu, Chandrajit Bajaj, and Wah Chiu. Applications of a bilateral denoising filter in biological electron microscopy. *Journal of Structural Biology*, 144(1):114–122, October 2003. (12)

[45] Peter van der Heide, Xiao-Ping Xu, Brad J. Marsh, Dorit Hanein, and Niels Volkmann. Efficient automatic noise reduction of electron tomographic reconstructions based on iterative median filtering. *Journal of Structural Biology*, 158(2):196–204, May 2007. (12)

[46] Dai-Yu Wei and Chang-Cheng Yin. An optimized locally adaptive nonlocal means denoising filter for cryo-electron microscopy data. *Journal of Structural Biology*, 172(3):211–218, December 2010. (12)

[47] Jaakko Lehtinen, Jacob Munkberg, Jon Hasselgren, Samuli Laine, Tero Karras, Miika Aittala, and Timo Aila. Noise2Noise: Learning Image Restoration without Clean Data. *arXiv:1803.04189 [cs, stat]*, October 2018. (13)

[48] Tim-Oliver Buchholz, Mareike Jordan, Gaia Pigino, and Florian Jug. Cryo-CARE: Content-Aware Image Restoration for Cryo-Transmission

Electron Microscopy Data. *arXiv:1810.05420 [cs]*, October 2018. (13, 16)

[49] Tristan Bepler, Kotaro Kelley, Alex J. Noble, and Bonnie Berger. Topaz-Denoise: General deep denoising models for cryoEM and cryoET. Preprint, Bioinformatics, November 2019. (13, 16)

[50] Tim Dahmen. *Tomographic Reconstruction of Combined Tilt- and Focal Series in Scanning Transmission Electron Microscopy*. PhD thesis, January 2015. (14)

[51] Kendra E. Leigh, Paula P. Navarro, Stefano Scaramuzza, Wenbo Chen, Yingyi Zhang, Daniel Castaño-Díez, and Misha Kudryashev. Subtomogram averaging from cryo-electron tomograms. In *Methods in Cell Biology*, volume 152, pages 217–259. Elsevier, 2019. (13)

[52] Yuxiang Chen and Friedrich Förster. Iterative reconstruction of cryo-electron tomograms using nonuniform fast Fourier transforms. *Journal of Structural Biology*, 185(3):309–316, March 2014. (13)

[53] Yuchen Deng, Yu Chen, Yan Zhang, Shengliu Wang, Fa Zhang, and Fei Sun. ICON: 3D reconstruction with 'missing-information' restoration in biological electron tomography. *Journal of Structural Biology*, 195(1):100–112, July 2016. (13)

[54] Michael Kunz and Achilleas S. Frangakis. Super-sampling SART with ordered subsets. *Journal of Structural Biology*, 188(2):107–115, November 2014. (13)

[55] A. S. Frangakis, J. Bohm, F. Forster, S. Nickell, D. Nicastro, D. Typke, R. Hegerl, and W. Baumeister. Identification of macromolecular complexes in cryoelectron tomograms of phantom cells. *Proceedings of the National Academy of Sciences*, 99(22):14153–14158, October 2002. (14)

[56] Zhou Yu and Achilleas S. Frangakis. Classification of electron subtomograms with neural networks and its application to template-matching. *Journal of Structural Biology*, 174(3):494–504, June 2011. (15, 16)

[57] Ali Punjani, John L. Rubinstein, David J. Fleet, and Marcus A. Brubaker. cryoSPARC: Algorithms for rapid unsupervised cryo-EM structure determination. *Nature Methods*, 14(3):290–296, March 2017. (15)

[58] Min Xu, Martin Beck, and Frank Alber. High-throughput subtomogram alignment and classification by Fourier space constrained fast volumetric matching. *Journal of Structural Biology*, 178(2):152–164, May 2012. (15)

[59] Antonio Martinez-Sanchez, Zdravko Kochovski, Ulrike Laugks, Johannes Meyer zum Alten Borgloh, Saikat Chakraborty, Stefan Pfeffer, Wolfgang Baumeister, and Vladan Lučić. Template-free detection and classification of membrane-bound complexes in cryo-electron tomograms. *Nat Methods*, January 2020. (15)

[60] Feng Wang, Huichao Gong, Gaochao Liu, Meijing Li, Chuangye Yan, Tian Xia, Xueming Li, and Jianyang Zeng. DeepPicker: A deep learning approach for fully automated particle picking in cryo-EM. *Journal of Structural Biology*, 195(3):325–336, September 2016. (15, 16)

[61] Dimitry Tegunov and Patrick Cramer. Real-time cryo-electron microscopy data preprocessing with Warp. *Nat Methods*, 16(11):1146–1152, November 2019. (15)

[62] Muyuan Chen, Wei Dai, Stella Y. Sun, Darius Jonasch, Cynthia Y. He, Michael F. Schmid, Wah Chiu, and Steven J. Ludtke. Convolutional Neural Networks for Automated Annotation of Cellular Cryo-Electron Tomograms. *Nat Methods*, 14(10):983–985, October 2017. (15, 16)

[63] Thorsten Wagner and Stefan Raunser. The evolution of SPHIRE-crYOLO particle picking and its application in automated cryo-EM processing workflows. *Commun Biol*, 3(1):61, December 2020. (15)

[64] Thorsten Wagner, Felipe Merino, Markus Stabrin, Toshio Moriya, Claudia Antoni, Amir Apelbaum, Philine Hagel, Oleg Sitsel, Tobias Raisch, Daniel Prumbaum, Dennis Quentin, Daniel Roderer, Sebastian Tacke, Birte Siebolds, Evelyn Schubert, Tanvir R. Shaikh, Pascal Lill, Christos Gatsogiannis, and Stefan Raunser. SPHIRE-crYOLO is a fast and accurate fully automated particle picker for cryo-EM. *Commun Biol*, 2(1):218, December 2019. (16)